Hydrol. Earth Syst. Sci. Discuss., 9, 13083–13115, 2012
www.hydrol-earth-syst-sci-discuss.net/9/13083/2012/
doi:10.5194/hessd-9-13083-2012
© Author(s) 2012. CC Attribution 3.0 License.

Hydrology and Earth System Sciences Discussions

This discussion paper is/has been under review for the journal Hydrology and Earth System Sciences (HESS). Please refer to the corresponding final paper in HESS if available.

Ensemble Kalman filter versus ensemble smoother for assessing hydraulic conductivity via tracer test data assimilation

E. Crestani[1], M. Camporese[1], D. Baú[2], and P. Salandin[1]

[1]Department of Civil, Environmental, and Architectural Engineering, University of Padova, Padova, Italy
[2]Department of Civil and Environmental Engineering, Colorado State University, Fort Collins, CO, USA

Received: 28 October 2012 – Accepted: 7 November 2012 – Published: 21 November 2012

Correspondence to: E. Crestani (elena.crestani@dicea.unipd.it)

Published by Copernicus Publications on behalf of the European Geosciences Union.

Abstract

The significance of estimating the spatial variability of the hydraulic conductivity K in natural aquifers is relevant to the possibility of defining the space and time evolution of a non-reactive plume, since the transport of a solute is mainly controlled by the heterogeneity of K. At the local scale, the spatial distribution of K can be inferred by combining the Lagrangian formulation of the transport with a Kalman filter-based technique and assimilating a sequence of time-lapse concentration C measurements, which, for example, can be evaluated on-site through the application of a geophysical method. The objective of this work is to compare the ensemble Kalman filter (EnKF) and the ensemble smoother (ES) capabilities to retrieve the hydraulic conductivity spatial distribution in a groundwater flow and transport modeling framework. The application refers to a two-dimensional synthetic aquifer in which a tracer test is simulated. Moreover, since Kalman filter-based methods are optimal only if each of the involved variables fit to a Gaussian probability density function (pdf) and since this condition may not be met by some of the flow and transport state variables, issues related to the non-Gaussianity of the variables are analyzed and different transformation of the pdfs are considered in order to evaluate their influence on the performance of the methods. The results show that the EnKF reproduces with good accuracy the hydraulic conductivity field, outperforming the ES regardless of the pdf of the concentrations.

1 Introduction

One of the most challenging tasks in groundwater flow and transport modeling is the assessment of hydraulic properties of the porous media such as the hydraulic conductivity (K), whose spatial heterogeneity is typically very pronounced in natural aquifers and thus particularly difficult to characterize. For this reason, many efforts have been made for the development of inverse models capable to estimate aquifer hydraulic properties at various scales. Extensive reviews of these methods have been provided by Carrera

HESSD
9, 13083–13115, 2012

EnKF vs. ES for tracer test data assimilation

E. Crestani et al.

et al. (1993); McLaughlin and Townley (1996); Zimmerman et al. (1998); Vrugt et al. (2008). Hydraulic conductivity and head data have been typically used to constrain inverse models (e.g. Chen and Zhang, 2006; Hendricks Franssen and Kinzelbach, 2008). More recently, the use of information derived by geophysical methods has been increasingly proposed and investigated for the estimation of parameters in groundwater modeling (e.g. Camporese et al., 2011; Pollock and Cirpka, 2012).

Among the several mathematical tools available for the inversion of hydrologic data, Bayesian methods such as the ensemble Kalman filter (EnKF) and its variations (Evensen, 2009b) allow for seeking an ensemble of independent samples conditional to the measurements, all representing equally likely realizations of the actual variability of the hydraulic parameters. These methods have been applied, for example, by: Chen and Zhang (2006), who used the EnKF to estimate the hydraulic conductivity both in two- and three-dimensional domains assimilating hydraulic head data and K measurements; Liu et al. (2008), who obtained the K distribution at the MADE site (e.g. Boggs et al., 1992) by assimilating, in two subsequent steps, hydraulic head and concentration data collected during a tracer test; and Bailey and Baú (2010), who used the ensemble smoother (ES) by assimilating hydraulic head and groundwater return flow volume measurements to estimate the hydraulic conductivity distribution in a synthetic two-dimensional case.

More recently, Hendricks Franssen et al. (2011) applied the EnKF to jointly calibrate the hydraulic conductivity and leakage coefficient in real-time in an unconfined aquifer. In Li et al. (2012), the EnKF was used to map the hydraulic conductivity and porosity fields by assimilating dynamic piezometric data and multiple concentration data. In Bailey and Baú (2012), the ES was iteratively applied to estimate the parameters of a geostatistical model through assimilation of water table elevation data. Tong et al. (2012) used the EnKF in a synthetic two-dimensional aquifer to estimate the hydraulic conductivity by assimilating solute concentration data measured in a large number of observation wells.

CC BY

Given the importance that EnKF and ES have gained in recent years as parameter estimation modeling tools in groundwater hydrology, there is the need to investigate in more detail their capabilities and the theoretical implications related to their use in a context that is much different from the one for which they were originally developed, i.e. the optimal estimation of system states only. The objective of this work is thus to compare the EnKF and ES capabilities to retrieve the hydraulic conductivity spatial distribution in a groundwater flow and transport modeling framework. Moreover, since a fundamental hypothesis for the application of Kalman filter-based methods is that all the variables must be distributed as a Gaussian probability density function (pdf), the issues related to various transformations of the relevant pdfs are analyzed. EnKF and ES are here implemented in the same Lagrangian transport modeling framework proposed by Crestani et al. (2010) and Camporese et al. (2011), in order to estimate the hydraulic conductivity field by assimilating concentration measurements derived from a tracer test in a two-dimensional synthetic aquifer. We hypothesize to follow the full spatio-temporal evolution of the solute plume, which may be obtained, for example, by means of electrical resistivity tomography experiments (e.g. Perri et al., 2012).

2 Theory and methods

2.1 The ensemble Kalman filter and the ensemble smoother

According to Evensen (2009a), the combined parameter and state estimation problem for a dynamical model can be formulated as finding the joint pdf of the parameters and model state, given a set of measurements and a dynamical model with known uncertainties. Using Bayes theorem, the problem can be written in the simplified form

$$f\left(\boldsymbol{y},\boldsymbol{\alpha}|z\right) = \gamma f\left(\boldsymbol{y},\boldsymbol{\alpha}\right) f\left(z|\boldsymbol{y},\boldsymbol{\alpha}\right), \tag{1}$$

where $f(\boldsymbol{y},\boldsymbol{\alpha})$ is the joint pdf for the model state $\boldsymbol{y}$ (as function of space and time) and the parameters $\boldsymbol{\alpha}$, $f(z|\boldsymbol{y},\boldsymbol{\alpha})$ is the likelihood function of the measurements z, and γ is

HESSD
9, 13083–13115, 2012

a normalization constant whose computation requires the evaluation of the integral of Eq. (1) over the multi-dimensional solution and parameter space. Note that in writing Eq. (1) we implicitly assume that the only uncertainty in the model formulation lies in the parameters, while boundary and initial conditions are perfectly known. If, as usual, we work with a model state that is discretized in time, we can represent $\boldsymbol{y}$ at fixed time intervals as $\boldsymbol{y}_i = \boldsymbol{y}(t_i)$ with $i = 0, 1, \ldots, k$. If we further assume that the model is a first-order Markov process, we can define the pdf for the model integration from time t_{i-1} to t_i as $f(\boldsymbol{y}_i|\boldsymbol{y}_{i-1}, \boldsymbol{\alpha})$. Let us now assume that also the measurements $\boldsymbol{z}$ can be divided into subsets of measurement vectors $\boldsymbol{z}_i$, collected at the same time steps of the model t_i and that the measurement errors are uncorrelated in time. Under these hypotheses and from Bayes theorem, Eq. (1) becomes (Evensen, 2009a)

$$f\left(\boldsymbol{y}_1, \ldots, \boldsymbol{y}_k, \boldsymbol{\alpha}|z\right) = \gamma f\left(\boldsymbol{\alpha}\right) \prod_{i=1}^{k} f\left(\boldsymbol{y}_i|\boldsymbol{y}_{i-1}, \boldsymbol{\alpha}\right) f\left(z_i|\boldsymbol{y}_i, \boldsymbol{\alpha}\right), \tag{2}$$

in which the pdf of the parameters $f(\boldsymbol{\alpha})$ is expressed explicitly. Rewriting (Eq. 2) as a sequence of iterations and integrating out the state variables at all previous times, we obtain

$$f\left(\boldsymbol{y}_i, \boldsymbol{\alpha}|z_1, \ldots, z_i\right) = \gamma f(\boldsymbol{\alpha}) f(\boldsymbol{y}_i|\boldsymbol{y}_{i-1}, \boldsymbol{\alpha}) f(z_i|\boldsymbol{y}_i, \boldsymbol{\alpha}). \tag{3}$$

The combined parameter and state estimation can thus be formulated sequentially using Bayesian statistics, under the condition that measurement errors are independent in time and the dynamical model is a Markov process. Equations (1) and (3) can be solved numerically by means of a Monte Carlo approach, which approximates the probabilistic information conveyed by the conditional pdfs of the state, parameters, and measurements with an ensemble of realizations of size NMC. Each of the NMC state vectors is propagated in time according to the forecast model, which can be expressed as a vector-valued discrete-time state equation:

$$\boldsymbol{y}^j(t) = A[\boldsymbol{y}^j(\tau), \boldsymbol{\alpha}^j, t, \tau]; \quad t_0 \le \tau < t; \quad \boldsymbol{y}^j(t_0) = \boldsymbol{y}_0^j, \tag{4}$$

HESSD
9, 13083–13115, 2012

where $\boldsymbol{y}^j(t)$ is the jth ($j = 1, \ldots,$NMC) state vector predicted by the model at the time t, $\boldsymbol{\alpha}^j$ is the jth set of model parameters, A is the operator relating the system state at the current time t to the system state at the previous time τ, and $\boldsymbol{y}_0^j$ is the initial condition at time t_0.

At time t_i, m_i measurements are available and the model describing how these measurements and the system state are related is also expressed as a vector-valued discrete-time measurement equation:

$$z^j(t_i) = \mathbf{H}\boldsymbol{y}_{\text{true}}(t_i) + \boldsymbol{w}^j(t_i), \tag{5}$$

where $\mathbf{H}$ is the operator that maps the model state to the measurements, $\boldsymbol{y}_{\text{true}}(t_i)$ is the true state, and $z^j(t_i)$ is the jth vector of observations at the time t_i, which is obtained perturbing the m_i measurements with a random noise $\boldsymbol{w}^j(t_i)$, representing the measurement errors. Here we assume that $\boldsymbol{w}^j(t_i)$ is normally distributed with expected value equal to zero and assigned variance σ^2_{meas}. Under the hypothesis that the pdfs for the model prediction as well as the likelihood are Gaussian, it is possible to update each realization of the system state according to the following equation, which is obtained by minimizing the model error covariance matrix (Evensen, 2009a):

$$\boldsymbol{y}^j_{\text{upd}} = \boldsymbol{y}^j + \mathbf{P}_\text{e}\mathbf{H}^T(\mathbf{H}\mathbf{P}_\text{e}\mathbf{H}^T + \mathbf{R}_\text{e})^{-1}(z^j - \mathbf{H}\boldsymbol{y}^j), \tag{6}$$

where $\boldsymbol{y}^j_{\text{upd}}$ is the jth realization of the updated system state, $\mathbf{P}_\text{e}$ is the prior estimate of the system state error covariance matrix, which is computed by sampling the ensemble statistics, and $\mathbf{R}_\text{e}$ is the measurement error covariance matrix.

Within the formulation of the ES, Eq. (1) requires that the pdfs are approximated from an integration of the ensemble through the whole assimilation time period. In other words, all of the data are processed by Eq. (6) in one step, and the solution is updated as a function of space and time, using the space-time covariances estimated from the ensemble of model realizations.

HESSD
9, 13083–13115, 2012

On the other hand, within the EnKF formulation, Eq. (3) is a sequential expression that can be solved through incremental updates given by Eq. (6) with the data at the current time step only.

Note that in both cases, when the model pdfs and the likelihood function are Gaussian, the Bayesian formulation corresponds to the minimization of a quadratic cost function (Evensen, 2009a). The only difference is that in ES the time dimension is included in the optimization, while in EnKF the minimization is performed at each assimilation time. However, when the pdfs are not Gaussian, Eq. (6) is an approximation and no longer yields optimal updates in terms of a cost function minimization, although the general Bayesian formulation remains valid, i.e. sampling of a posterior pdf is still performed.

2.2 The inversion model

The Lagrangian approach described in Dagan (1989) is here adopted to describe the movement of a tracer plume through a saturated, spatially heterogeneous porous medium. As described in Crestani et al. (2010) and Camporese et al. (2011), the solute cloud is driven by the effective velocity field obtained at steady state solving the groundwater flow equation with appropriate boundary conditions. In natural sedimentary aquifers the spatial variability of the porosity ϕ can be considered negligible with respect to that of K (e.g. Gelhar, 1993), so that the concentration C, related to the pdf of the Lagrangian trajectory of equation $\boldsymbol{x} = \boldsymbol{X}_t(t;\boldsymbol{a},t_0)$, where $\boldsymbol{a}$ is the initial position of the considered particle and t_0 the injection time, is fully controlled by the spatial distribution of the hydraulic conductivity. Dealing with real applications, our interest is related to the average concentration C over a finite volume ΔV whose centroid is at $\boldsymbol{x}$. By defining as $M = \phi C_0 V_0$ the total mass of initial concentration C_0 uniformly injected in the volume V_0, an estimation of the concentration value is given by:

Discussion Paper | Discussion Paper | Discussion Paper | Discussion Paper |

HESSD

9, 13083–13115, 2012

EnKF vs. ES for tracer test data assimilation

E. Crestani et al.

$$C(\boldsymbol{x},t;t_0) = \frac{\phi}{M}\int_{\Delta V}\int_{V_0} C_0(\boldsymbol{a})\delta[\boldsymbol{x}' - \boldsymbol{X}_t(t;\boldsymbol{a},t_0)]\mathrm{d}\boldsymbol{a}\,\mathrm{d}\boldsymbol{x}'$$
$$= \frac{1}{N\Delta V}\int_{\Delta V}\sum_{i=1}^{N}\delta[\boldsymbol{x}' - \boldsymbol{X}_t(t;\boldsymbol{a},t_0)]\Delta\boldsymbol{a}\,\mathrm{d}\boldsymbol{x}', \tag{7}$$

where N is the number of particles released to simulate the solute and δ is the Dirac delta function.

The problem of estimating the hydraulic conductivity field by using concentration measurements is solved by considering a system state in which we retain only the model parameters:

$$\boldsymbol{y}^j = [Y_1, \ldots, Y_n]^j = \boldsymbol{\alpha}^j, \tag{8}$$

where $Y_1, \ldots, Y_n$ are the log-transformed hydraulic conductivity values ($Y = \ln K$) at the n nodes discretizing the domain. At time t_0, NMC realizations of the log-transformed hydraulic conductivity field are generated from a prior $f(\boldsymbol{\alpha})$ and the state vectors are built as in Eq. (8).

In the EnKF application, starting with the the same initial concentration C_0 for each Y field, the solute plume is propagated forward in time to the first measurement time t_1, using the Lagrangian transport model. At time t_1 the log-transformed hydraulic conductivities $(Y_1, \ldots, Y_n)^j$ are updated based on the m_1 measurements available by means of Eq. (6), which leverages to the cross-correlation between Y and C, expressed by the product $\mathbf{P}_\mathrm{e}\mathbf{H}^T$. The process continues sequentially: first a propagation step over each interval between t_0 and t_i and then an update step of the log-transformed hydraulic conductivity values at each measurement time t_i. The process stops at the time corresponding to the last measurement t_{tm}. It must be observed that, in order to ensure mass conservation throughout the simulation, after every assimilation step the plume evolves in the updated Y fields starting from t_0 and with the same initial solute

HESSD
9, 13083–13115, 2012

cc BY

distribution. This recursive application of the EnKF differs from the classic sequential one commonly adopted, since by restarting the plume evolution with the same initial concentration in updated Y fields, we apply the predictive analysis expressed by the Kalman gain on a system state that is improved at each assimilation step.

In the ES application, there is no need for sequential updates and the parameters are estimated in a single off-line step. At time t_0, each realization of the ensemble of NMC Y fields is initialized with the same concentration distribution C_0 and the solute plume is propagated forward in time until the last assimilation time, and the concentration distributions for all measurement times are recorded. The measurement vectors are thus assembled as

$$z^j = [z(t_1), z(t_2), \ldots, z(t_{\mathrm{tm}})]^{j^T}, \tag{9}$$

i.e. the perturbed measurements for all the measurement times (tm) are stored in a vector of dimension $[\sum_{i=1}^{\mathrm{tm}} m_i]$, for each Monte Carlo simulation. Since the ES does not require sequential updates, the computational time is expected to be significantly lower than in the EnKF, even though the dimension of the vectors and matrices in Eq. (6) is significantly larger than in EnKF.

For both EnKF and ES, the numerical computation of the update step implemented in this study follows the square root algorithm developed by Evensen (2004).

3 Numerical experiments

3.1 Model setup

A two-dimensional reference Y field is considered to compare the proposed inversion models in a number of numerical experiments. The domain has dimensions of $8\,\mathrm{L} \times 8\,\mathrm{L}$, where L is an arbitrary and consistent unit length, and it is discretized along each direction into L/4 sided cells, for a total of $33 \times 33 = 3297$ corresponding nodes. By assuming $Y = \ln(K)$, the multivariate normal Y distribution of the reference field is the

HESSD
9, 13083–13115, 2012

result of a single unconditional generation conforming to an isotropic exponential covariance model with spatial mean $\langle Y \rangle = 0.35$, variance of $\sigma_Y^2 = 0.42$, and integral scale $\lambda = 1\,\mathrm{L}$. The random function Y is generated by an improved sequential Gaussian simulation algorithm (Baú and Mayer, 2008). The flow field is simulated using a standard finite volume solver at steady state with appropriate boundary conditions that ensure a constant mean gradient. The resulting Eulerian velocity field is used for the computation of the trajectories of N particles suitable for the simulation of a contaminant release. Dirichlet boundary conditions are applied at $x = 0\,\mathrm{L}$ ($h = 100.0\,\mathrm{L}$) and at $x = 8\,\mathrm{L}$ ($h = 95.2\,\mathrm{L}$), while Neumann no-flow boundary conditions are imposed along the remaining sides of the domain. A graphic representation of the reference field is given in Fig. 1. A tracer test is simulated by assuming an instantaneous solute injection with initial transversal size of $6\,\mathrm{L}$ (from $y = 1\,\mathrm{L}$ to $y = 7\,\mathrm{L}$) and longitudinal size of $0.5\,\mathrm{L}$ (centered in $x = 0.875\,\mathrm{L}$). The solute is simulated by 16983 particles uniformly distributed, with the particle trajectories computed by means of the Pollock's particle tracking post-processing algorithm (Salandin et al., 2000) and the concentration computed according to Eq. (7) every $0.5\,\mathrm{T}$, where T is any consistent time unit. Figure 2 shows the plume evolution in the reference field at $t = 2\,\mathrm{T}$ and $t = 4\,\mathrm{T}$.

In this work, the inversion is carried out by assimilating concentration data. In particular, we include in the measurement vectors all the concentration data greater than zero, in order to use all the available information on the plume evolution. The performances of EnKF and ES in retrieving the Y fields are compared to one another in a number of different scenarios described in Table 1. In these scenarios we also analyze the implications of the concentration non-Gaussianity through various transformations of the pdf. The prior geostatistical parameters and the measurement uncertainty are kept constant in all scenarios, as the objective is to study the issues related to the effect of the pdf of the model variables on the EnKF and the ES performances in terms of parameter estimation. In scenario 1 the concentration data are assimilated without any transformation, i.e. with their original pdf, whereas in scenarios 2, 3, and 4 different pdf transformations are used to evaluate how they affect the parameter estimation by

HESSD
9, 13083–13115, 2012

CC BY

approaching the Gaussian requirement. Based on preliminary sensitivity analyses, all scenarios are simulated using an ensemble size of 2000. This number of realizations is computationally affordable and guarantees a proper description of the dispersion process for the range of log-transformed hydraulic conductivity variance used here (Bellin et al., 1992; Salandin and Fiorotto, 1998).

It should be noted that the ensemble of prior Y fields is synthetically generated by the same algorithm used to create the true field and that the application of the Lagrangian transport model in the true field yields exactly the true concentration distribution. The knowledge of the true state allows us to select the concentration measurements used during the assimilation and to evaluate the performance of EnKF and ES with respect to a known reference.

The estimate of the hydraulic conductivity fields in the various simulated scenarios is assessed by means of the root mean square error (RMSE) of the ensemble mean, computed as

$$\mathrm{RMSE} = \sqrt{\frac{\sum_{i=1}^{n}(Y_{\mathrm{sim},i} - Y_{\mathrm{true},i})^2}{n}}, \tag{10}$$

where n is the total number of nodes of the discretized domain, $Y_{\mathrm{sim},i}$ is the ensemble mean of the Y values estimated at the ith node, and $Y_{\mathrm{true},i}$ is the true Y value at the ith node.

Finally, we also assess the plume evolution as simulated in the reconstructed Y fields by means of the concentration RMSE, whose formulation is analogous to that of Y.

3.2 Results

3.2.1 Scenarios with untransformed concentration pdfs

In scenarios 1a and 1b, the concentration values are assimilated in the update procedure without modifying their original pdf, for both the EnKF and the ES. The spatial

HESSD
9, 13083–13115, 2012

CC BY

distributions of Y resulting from the inversions are reported in Fig. 3. The comparison between the retrieved fields and the reference field (Fig. 1) shows that the EnKF is quite effective in estimating the $\ln K$ field, whereas the ES performs rather poorly.

In these scenarios, both EnKF and ES are affected by the approximations related to the Gaussian assumption of Eq. (6), as the tracer concentration pdf at early travel times departs significantly from the normal pdf (e.g. Salandin and Fiorotto, 1998). Nevertheless, EnKF can handle these approximations better than ES, as, at each update, the realizations are steered toward the true solution and the Gaussian increments of the ensemble members lead to an approximately Gaussian ensemble distributed around the true solution. This property of the sequential updating is not exploited in the ES, where realizations evolve freely until the end of the simulation, exacerbating the effects related to non-Gaussian ensemble distributions. A further explanation for the good performance of the EnKF can be found in our recursive application, through which, at each assimilation step, the plume is restarted with the same initial concentration in the updated Y fields. This procedure is analogous to the advanced first-order second-moment (AFOSM) method adopted in risk analysis (Yen et al., 1986). As in AFOSM, also in our EnKF application the lack of Gaussianity is overcome by approaching recursively the solution with improved values of the estimator (the Kalman gain) corresponding to improved estimates of the solution itself.

3.2.2 Scenarios with log-transformed concentration pdfs

In order to evaluate if a proper rearrangement of the concentration pdf can improve the results, in scenarios 2a and 2b we assimilate log-transformed concentration values. Although previous analyses highlight that Beta-type pdfs can be effectively used to reproduce the concentration distribution (Caroni and Fiorotto, 2005), the log-normal pdf is easier to handle and often represents a reasonable assumption (e.g. Bellin et al., 1994; Zhang et al., 2000).

Figure 4 shows the Y fields estimated by EnKF and ES when assimilating log-transformed concentration measurements. The EnKF produces again a good

HESSD
9, 13083–13115, 2012

EnKF vs. ES for tracer test data assimilation

E. Crestani et al.

CC BY

reproduction of the true hydraulic conductivity field, with only small differences compared to the results of scenario 1a, while the ES confirms its difficulty in retrieving the Y spatial distribution. Nonetheless, the comparison between scenarios 1b and 2b shows a slight improvement of the ES solution, indicating that the ES is more sensitive than the EnKF to the pdf of the assimilated variable.

3.2.3 Scenarios with normal score-transformed concentration pdfs

Since the log-transformation of concentration values does not ensure a normal pdf in all cases, in scenarios 3a and 3b another type of transformation is applied to the concentration data. Here a Gaussian pdf of the C values is obtained by applying a normal score transform (NST) (Zhou et al., 2011). The NST is a tool through which any cumulative probability distribution function (CDF) $F(x)$ is mirrored to the standard Gaussian CDF $G(y)$. In other words, the generic variable x of the $F(x)$ distribution can be transformed into the corresponding normally distributed variable y through the relation $F(x) = G(y)$, i.e. $y = G^{-1}[F(x)]$. In this case $x = C$ and a CDF is built for each node of the domain with the ensemble of C values simulated by the model, using the Hazen formula $F(C) = (i - 0.5)/\mathrm{NMC}$, where $i = 1,...,\mathrm{NMC}$ is the rank of the concentration values after sorting the data in ascending order. For each node, different values of C are univocally associated to the CDF values, which are always the same and depend only on NMC.

The results obtained by assimilating normal score-transformed concentration data are reported in Fig. 5 for both EnKF and ES. Despite the Gaussian distribution of the model variables, the retrieved fields are not satisfactory for both the techniques and, compared to the results of scenarios 1a and 2a, even the EnKF performs poorly.

Since in scenario 3 the approximations related to the Gaussian assumption are removed, the results seem to suggest that the NST might corrupt the cross-correlation structure between Y and C in the measurement locations. Indeed, when the C values are log-transformed, the relation that maps the original pdf of C to the transformed one is the same for all the different positions in space and thus the correlation structure is

HESSD
9, 13083–13115, 2012

CC BY

conserved. This is not the case for scenario 3, where a different NST is independently applied to the concentration ensemble at each node.

In order to illustrate this point, the $C-Y$ cross-correlation structures, evaluated in the measurement nodes by means of the product $\mathbf{PH}^T$ in Eq. (6), are compared for scenarios 1 and 3. The cross-correlation structures for scenario 1 at time $t = 2\mathrm{T}$ and $t = 4\mathrm{T}$ are reported in panels a and b of Figs. 6 and 7, respectively, while panels c and d of the same Figures refer to scenario 3. The analysis considers only the longitudinal behavior of the cross-correlation, by reporting in the figures only the results calculated along the direction shown with a dotted line in Fig. 2. Firstly, we note that there are relevant differences between the EnKF and ES cross-correlation structures. The EnKF cross-correlation behavior shows always higher values at the origin (zero lag) and a rapid decay with increasing lag, i.e. moving away from the measurement location. This confirms that the effectiveness of the EnKF is limited in a portion of the domain around the measurement location (Camporese et al., 2011). With ES, the peak of correlation at the measurement location is usually smaller than with EnKF, and the cross-correlation structure is more spread out. As the cross-correlation between Y and C is usually significant only for a limited lag distance, proportional to the product of the Y integral scale and the length of the area covered by the plume, the relatively high correlation values characterizing the ES results at large lags are probably spurious. Also for this reason the result of the ES inversion is a smoothed Y field. Secondly, when the NST is applied (compare panels c and d with a and b in Figs. 6 and 7), there is an overall decrease of the peaks and the cross-correlation structures are even more smoothed, showing the significant alterations caused by the transformation.

3.2.4 Scenarios with modified normal score-transformed concentration pdfs

In order to maintain the original Y–C cross-correlation structure and, at the same time, to work with Gaussian pdfs, a modified application of the NST is proposed. At every time step, only one cumulative distribution function is built by using the concentration values simulated in all the measurement nodes. We underline that this is different from the previous application of the NST, in which a relation between C and its CDF is defined in each node independently. Now the CDF $F(C)$, estimated at time t_i, is $F(C) = (i - 0.5)/(\mathrm{NMC} \times m_i)$, where m_i is the number of measurement locations and $i = 1, \ldots, \mathrm{NMC} \times m_i$ is the rank of the concentration values after sorting the data in ascending order. With this modified application of the NST we obtain a satisfactory reproduction of the Gaussian distribution in each node, and, by using an invariant transformation, we do not alter the Y–C cross-correlation structure.

The results of the inversions, reported in Fig. 8 for both EnKF and ES, demonstrate the effectiveness of the modified NST, as the estimated Y fields are now showing an improvement (with respect to the prior fields) comparable to that in scenario 2 and look better than those of scenario 3. As in the previous scenarios, EnKF outperforms ES, which, however, shows significant improvements and seems to benefit more from the application of the modified NST.

3.3 Discussion

In Fig. 9, the results of all the scenarios are summarized and compared in terms of root mean square errors of both Y and C vs. time. All of the observations made in the previous sections, which were based merely on visual comparison, are confirmed by the RMSE profiles. The EnKF consistently outperforms the ES, regardless of the adopted concentration pdfs, except for scenario 3a, in which the NST deteriorates the EnKF solution due to alterations of the Y–C cross-correlation structure. This result, which reveals the inadequacy of the NST for this application, is in accordance with the conclusions drawn by Schöniger et al. (2012). In their work, Schoeniger et al. applied the NST in conjunction with the EnKF to assimilate aquifer drawdown measurements and showed that the dependence between these data and the parameters is higher than the one between concentrations and parameters. The ES is more sensitive to the transformations applied to the assimilated data, as indicated by the RMSE of Y in the various scenarios, even though the same sensitivity is not reflected by the C RMSE (Fig. 9).

HESSD
9, 13083–13115, 2012

Overall, the problem of retrieving the hydraulic conductivity field through the assimilation of concentration measurements is better handled by EnKF, due to the violation of Gaussianity investigated earlier with the different scenarios and to the high nonlinearity of the problem under consideration. With EnKF, the Y fields are progressively updated and the simulated plumes gradually converge towards the true one. With ES, the plumes evolve freely in the prior fields until the end of the simulation and, consequently, their evolution is very different from the true one, especially at late times. To highlight this point, the true plume evolution at $t = 2\mathrm{T}$ and $t = 4\mathrm{T}$ (Fig. 2) is compared with the evolution of the ensemble mean of the plumes simulated in the prior fields (Fig. 10). In Figs. 11 and 12 we also show the evolution of the ensemble average of the plumes as simulated in the Y fields estimated at $t = 2\mathrm{T}$ and $t = 4\mathrm{T}$, respectively, in scenario 1a (EnKF with original concentration pdfs). In other words, in Fig. 11 EnKF is applied only until $t = 2\mathrm{T}$ and thereafter the plumes are let to evolve in the estimated Y fields. The progressive correction of the mean simulated plume is evident and already at $t = 2\mathrm{T}$ it is very similar to the true one. With ES, instead, there are no recursive updates that modify the ensemble to resemble the true Y field and the nonlinearity of the problem cannot be captured.

4 Summary and conclusions

The present work investigated the capabilities of the EnKF and the ES to retrieve the hydraulic conductivity spatial distribution through the assimilation of concentration measurements. The objective was to compare the performance of the two techniques and to analyze the effects of the lack of Gaussianity in the system variables. A tracer injection was simulated in a two-dimensional domain representing a heterogeneous aquifer and different scenarios were analyzed to determine how different transformations of the concentration probability distribution impact on the inversion results. In the first scenarios the concentrations were assimilated in the model without any manipulation, while in the other scenarios we took into account log-transformed data and two variants of the

HESSD
9, 13083–13115, 2012

normal score transform (NST), analyzing also the cross-correlation structure between log-transformed hydraulic conductivity Y and concentration C.

The main conclusion of our study is that EnKF can reproduce with good accuracy the hydraulic conductivity field, consistently outperforming ES regardless of the probability distribution of the concentrations. This is due to two reasons: (i) the lack of Gaussianity is overcome owing to the recursive Gaussian increments given by the EnKF updates that eventually lead to an ensemble of members normally distributed around the true solution; (ii) the same recursive procedure continuously pulls the realizations toward the true solution, easing the inversion problem of the strong nonlinearity of the dispersion process. The only case in which EnKF does not work properly is when NST is applied to ensure that the concentration pdf is Gaussian in each node of the domain. This is due to the consequent alteration of the Y–C cross-correlation structure, which instead must be correctly evaluated in order to assure the effectiveness of the EnKF inversion procedure. This suggests that NST must be applied with caution in any Kalman-filter based inversion scheme, checking at any time for possible corruptions of the cross-correlation between parameters and assimilation variables.

ES performs always worse than EnKF as it does not involve recursive updates of the Y fields. This has two consequences: (i) the solute plumes are free to evolve in the prior fields without corrections, eventually leading to significant differences from the true plume evolution; (ii) non-Gaussian contributions in the concentration pdf are not kept under control.

Acknowledgements. This work was supported by the University of Padova (projects CPDA089375 and STPD08RWBY).

HESSD
9, 13083–13115, 2012

CC BY

References

Bailey, R. and Baú, D.: Ensemble smoother assimilation of hydraulic head and return flow data to estimate hydraulic conductivity distribution, Water Resour. Res., 46, W12543, doi:10.1029/2010WR009147, 2010. 13085

Bailey, R. T. and Baú, D.: Estimating geostatistical parameters and spatially-variable hydraulic conductivity within a catchment system using an ensemble smoother, Hydrol. Earth Syst. Sci., 16, 287–304, doi:10.5194/hess-16-287-2012, 2012. 13085

Baú, D. and Mayer, A.: Optimal design of pump-and-treat systems under uncertain hydraulic conductivity and plume distribution, J. Contam. Hydrol., 100, 30–46, doi:10.1016/j.jconhyd.2008.05.002, 2008. 13092

Bellin, A., Salandin, P., and Rinaldo, A.: Simulation of dispersion in heterogeneous porous formations: statistics, first order theories, convergence of computations, Water Resour. Res., 28, 2211–2227, doi:10.1029/92WR00578, 1992. 13093

Bellin, A., Rubin, Y., and Rinaldo, A.: Eulerian-Lagrangian approach for modeling of flow and transport in heterogeneous geological formations, Water Resour. Res., 30, 2913–2924, doi:10.1029/94WR01489, 1994. 13094

Boggs, J., Young, S., Beard, L., Gelhar, L., Rehfeldt, K., and Adams, E.: Field study of dispersion in a heterogeneous aquifer: 1. Overview and site description, Water Resour. Res., 28, 3281–3291, doi:10.1029/92WR01756, 1992. 13085

Camporese, M., Cassiani, G., Deiana, R., and Salandin, P.: Assessment of local hydraulic properties from electrical resistivity tomography monitoring of a three-dimensional syntetic tracer test experiment, Water Resour. Res., 47, W12508, doi:10.1029/2011WR010528, 2011. 13085, 13086, 13089, 13096

Caroni, E. and Fiorotto, V.: Analysis of concentration as sampled in natural aquifers, Transport Porous Med., 59, 19–45, doi:10.1007/s11242-004-1119-x, 2005. 13094

Carrera, J., Medina, A., and Galarza, G.: Groundwater inverse problem: discussion on geostatistical formulations and validation, Hydrogeologie, 4, 313–324, 1993. 13084

Chen, Y. and Zhang, D.: Data assimilation for transient flow in geologic formations via ensemble Kalman filter, Adv. Water Resour., 29, 1107–1122, doi:10.1016/j.advwatres.2005.09.007, 2006. 13085

CC BY

Crestani, E., Camporese, M., and Salandin, P.: Hydraulic conductivity assessment via tracer test data assimilation: a comparison of updating techniques, in: Proceedings of the IAHR International Groundwater Symposium 2010, p. 4, Valencia, Spain, 2010. 13086, 13089

Dagan, G.: Flow and Transport in Porous Formations, Springer, New York, 1989. 13089

Evensen, G.: Sampling strategies and square root analysis schemes for the EnKF, Ocean Dynam., 54, 539–560, doi:10.1007/s10236-004-0099-2, 2004. 13091

Evensen, G.: The ensemble Kalman filter for combined state and parameter estimation, IEEE Contr. Syst. Mag., 29, 83–104, doi:10.1109/MCS.2009.932223, 2009a. 13086, 13087, 13088, 13089

Evensen, G.: Data Assimilation. The Ensemble Kalman Filter, Springer, New York, 2009b. 13085

Gelhar, L.: Stochastic Subsurface Hydrology, Prentice Hall, Englewood Cliff, NY, 1993. 13089

Hendricks Franssen, H. J. and Kinzelbach, W.: Real-time groundwater flow modeling with the Ensemble Kalman Filter: joint estimation of states and parameters and the filter inbreeding problem, Water Resour. Res., 44, 1–21, doi:10.1029/2007WR006505, 2008. 13085

Hendricks Franssen, H. J., Kaiser, H. P., Kuhlmann, U., Bauser, G., Stauffer, F., Muller, R., and Kinzelbach, W.: Operational real-time modeling with ensemble Kalman filter of variably saturated subsurface flow including stream-aquifer interaction and parameter updating, Water Resour. Res., 47, W02532, doi:10.1029/2010WR009480, 2011. 13085

Li, L., Zhou, H., Gomez-Hernandez, J. J., and Franssen, H. J. H.: Jointly mapping hydraulic conductivity and porosity by assimilating concentration data via ensemble Kalman filter, J. Hydrol., 428, 152–169, doi:10.1016/j.jhydrol.2012.01.037, 2012. 13085

Liu, G., Chen, Y., and Zhang, D.: Investigation of flow and transport processes at the MADE site using ensemble Kalman filter, Adv. Water Resour., 31, 975–986, doi:10.1016/j.advwatres.2008.03.006, 2008. 13085

McLaughlin, D. and Townley, L. R.: A reassessment of the groundwater inverse problem, Water Resour. Res., 32, 1131–1161, doi:10.1029/96WR00160, 1996. 13085

Perri, M., Cassiani, G., Gervasio, I., Deiana, R., and Binley, A.: A saline tracer test monitored via both surface and cross-borehole electrical resistivity tomography: comparison of time-lapse results, J. Appl. Geophys., 79, 6–16, doi:10.1016/j.jappgeo.2011.12.011, 2012. 13086

Pollock, D. and Cirpka, O.: Fully coupled hydrogeophysical inversion of a laboratory salt tracer experiment monitored by electrical resistivity tomography, Water Resour. Res., 48, W01505, doi:10.1029/2011WR010779, 2012. 13085

HESSD

9, 13083–13115, 2012

EnKF vs. ES for tracer test data assimilation

E. Crestani et al.

Salandin, P. and Fiorotto, V.: Solute transport in highly heterogeneous aquifers, Water Resour. Res., 34, 949–961, doi:10.1029/98WR00219, 1998. 13093, 13094

Salandin, P., Fiorotto, V., and Deppo, L. D.: Particle's tracking in 3-D heterogeneous porous media transport models, in: Computational Methods, Surface Water System and Hydrology, edited by: Bentley, L., Sykes, J., Brebbia, C., Gray, W., and Pinder, G., Balkema, Rotterdam, The Netherlands, 813–818, 2000. 13092

Schöniger, A., Nowak, W., and Hendricks, H. F.: Parameter estimation by ensemble Kalman filters with transformed data: approach and application to hydraulic tomography, Water Resour. Res., 48, W04502, doi:10.1029/2011WR010462, 2012. 13097

Tong, J., Hu, B. X., and Yang, J.: Data assimilation methods for estimating a heterogeneous conductivity field by assimilating transient solute transport data via ensemble Kalman filter, Hydrol. Process., online first: doi:10.1002/hyp.9523, 2012. 13085

Vrugt, J. A., Stauffer, P. H., Wöhling, T., Robinson, B. A., and Vesselinov, V. V.: Inverse modeling of subsurface flow and transport properties: a review with new developments, Vadose Zone J., 7, 843–864, doi:10.2136/vzj2007.0078, 2008. 13085

Yen, B., Cheng, A., and Melching, C.: First order reliability analysis, in: Stochastic and Risk Analysis in Hydraulic Engineering, Water Resources Publications, iSBN 0918334-57-8, 1986. 13094

Zhang, D., Andricevic, R., Sun, A., Hu, X., and He, G.: Solute flux approach to transport through spatially nonstationary flow in porous media, Water Resour. Res., 36, 2107–2120, doi:10.1029/2000WR900085, 2000. 13094

Zhou, H., Gómez-Hernández, J. J., Hendricks Franssen, H.-J., and Li, L.: An approach to handling non-Gaussianity of parameters and state variables in ensemble Kalman filtering, Adv. Water Resour., 34, 844–864, doi:10.1016/j.advwatres.2011.04.014, 2011. 13095

Zimmerman, D. A., de Marsily, G., Gotway, C. A., Marietta, M. G., Axness, C. L., Beauheim, R. L., Bras, R. L., Carrera, J., Dagan, G., Davies, P. B., Gallegos, D. P., Galli, A., Gomez-Hernandez, J., Grindrod, P., Gutjahr, A. L., Kitanidis, P. K., Lavenue, A. M., McLaughlin, D., Neuman, S. P., RamaRao, B. S., Ravenne, C., and Rubin, Y.: A comparison of seven geostatistically based inverse approaches to estimate transmissivities for modeling advective transport by groundwater flow, Water Resour. Res., 34, 1373–1413, doi:10.1029/98WR00003, 1998. 13085

Table 1. Description, prior geostatistical parameters, and measurement errors of the numerical experiments.

	assimilated data	technique	prior statistics $< Y >$	σ_Y^2	λ (L)	CV[a]
Reference field	–	–	0.03	0.43	1	–
Scenario 1a	C	EnKF	−0.50	0.75	1	0.01
Scenario 1b	C	ES	−0.50	0.75	1	0.01
Scenario 2a	lnC	EnKF	−0.50	0.75	1	0.01
Scenario 2b	lnC	ES	−0.50	0.75	1	0.01
Scenario 3a	NST(C)[b]	EnKF	−0.50	0.75	1	0.01
Scenario 3b	NST(C)[b]	ES	−0.50	0.75	1	0.01
Scenario 4a	modNST(C)[c]	EnKF	−0.50	0.75	1	0.01
Scenario 4b	modNST(C)[c]	ES	−0.50	0.75	1	0.01

[a] Measurement coefficient of variation.
[b] Normal score transform applied independently to the ensemble of concentration data in each assimilation node.
[c] Normal score transform applied to the ensemble of concentration data over all assimilation nodes.

Discussion Paper | Discussion Paper | Discussion Paper | Discussion Paper |
HESSD
9, 13083–13115, 2012

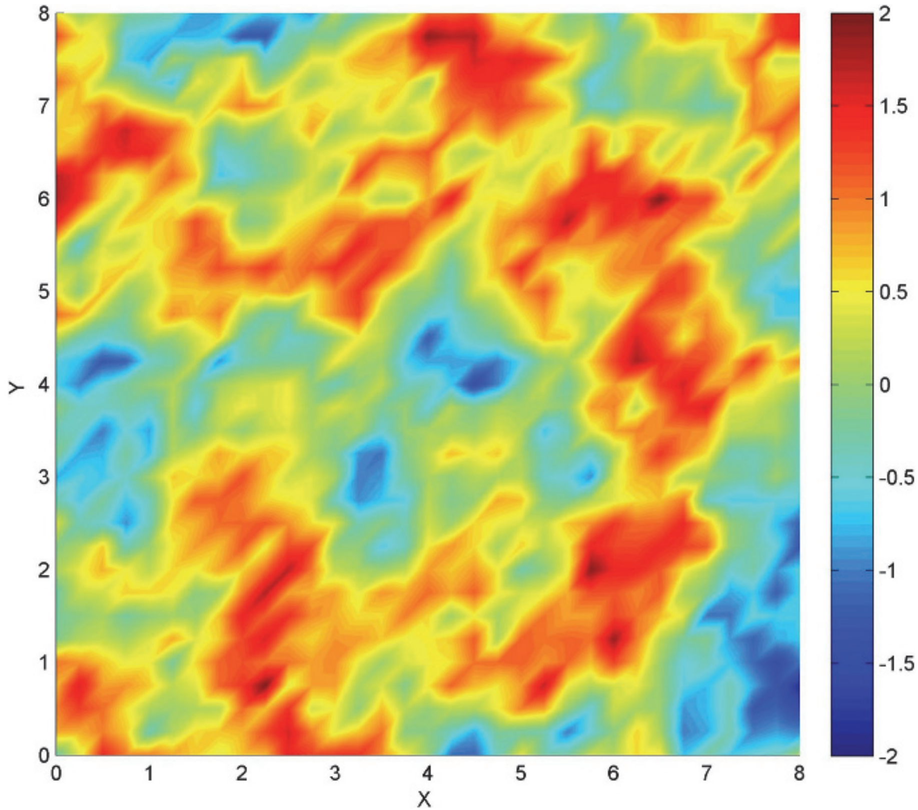

Fig. 1. Spatial distribution of log-transformed hydraulic conductivity in the reference field. The color bar indicates log-transformed hydraulic conductivity Y in $\ln(\mathrm{L\,T^{-1}})$.

HESSD
9, 13083–13115, 2012

EnKF vs. ES for tracer test data assimilation

E. Crestani et al.

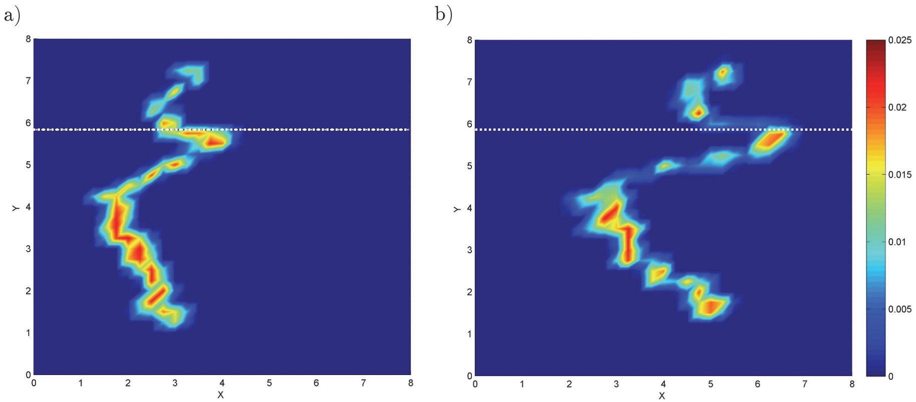

Fig. 2. Plume evolution in the reference field at **(a)** $t = 2\,\mathrm{T}$ and **(b)** $t = 4\,\mathrm{T}$. The color bar denotes dimensionless concentration C. Dotted lines show the direction along which the cross-correlation structure between Y and C is evaluated.

HESSD
9, 13083–13115, 2012

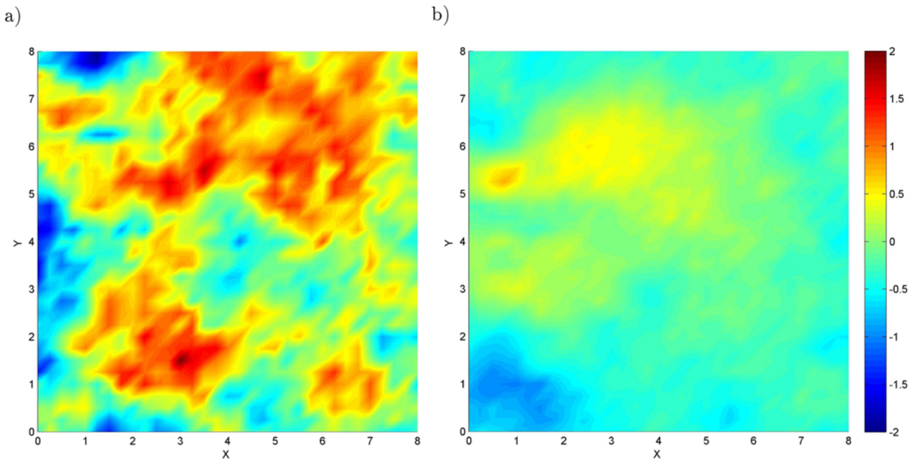

Fig. 3. Scenario 1: log-transformed hydraulic conductivity field retrieved by **(a)** EnKF and **(b)** ES assimilating untrasformed concentration data. The color bar indicates log-transformed hydraulic conductivity in $\ln(\mathrm{L\,T^{-1}})$.

HESSD
9, 13083–13115, 2012

EnKF vs. ES for tracer test data assimilation

E. Crestani et al.

CC BY

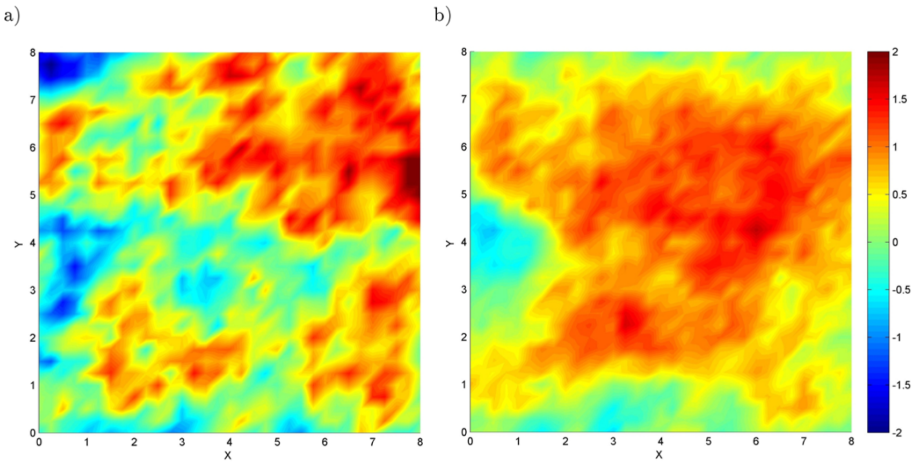

Fig. 4. Scenario 2: log-transformed hydraulic conductivity field retrieved by **(a)** EnKF and **(b)** ES assimilating log-transformed concentration data. The color bar indicates log-transformed hydraulic conductivity in $\ln(\mathrm{L\,T^{-1}})$.

HESSD
9, 13083–13115, 2012

CC BY

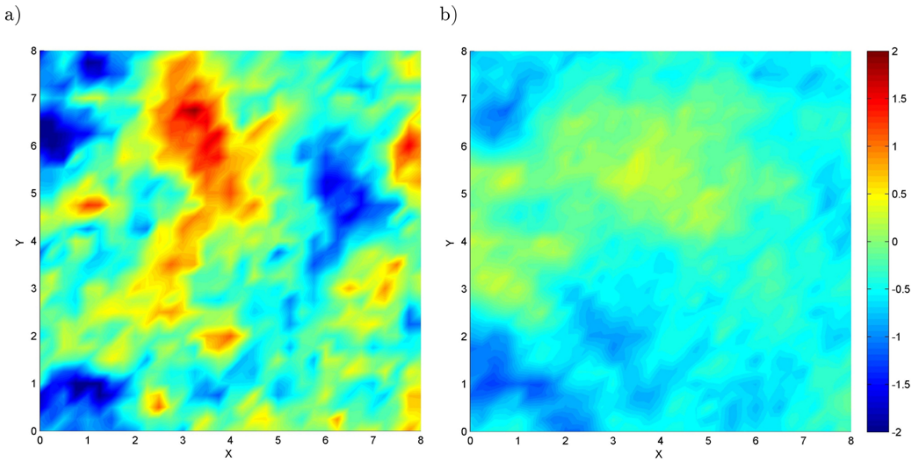

Fig. 5. Scenario 3: log-transformed hydraulic conductivity field retrieved by **(a)** EnKF and **(b)** ES assimilating normal score-transformed concentration data. The color bar indicates log-transformed hydraulic conductivity in $\ln(\mathrm{L\,T^{-1}})$.

HESSD
9, 13083–13115, 2012

EnKF vs. ES for tracer test data assimilation

E. Crestani et al.

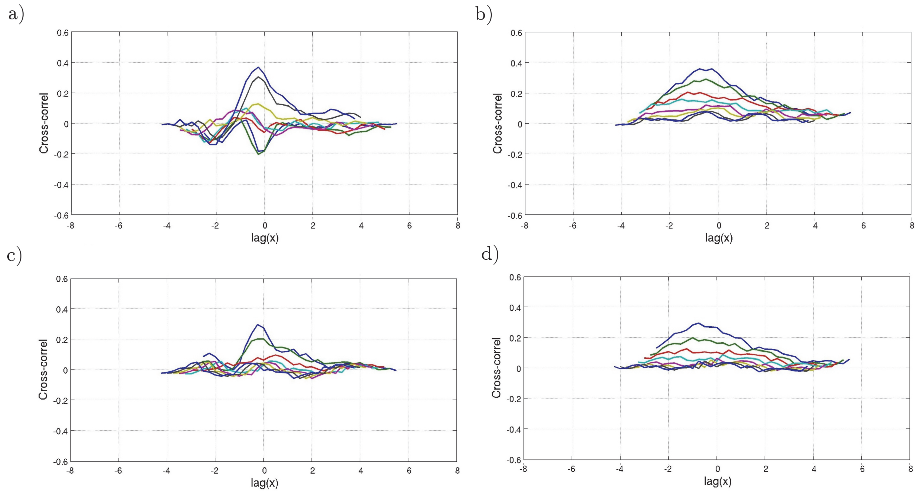

Fig. 6. Y–C cross-correlation at $t = 2\mathrm{T}$ for the nodes located at $y = 5.75\,\mathrm{L}$ in scenario 1a **(a)**, scenario 1b **(b)**, scenario 3a **(c)** and scenario 3b **(d)**. Each color corresponds to a correlation structure centered at a different node sampled by the plume (see Fig. 2a).

HESSD
9, 13083–13115, 2012

CC BY

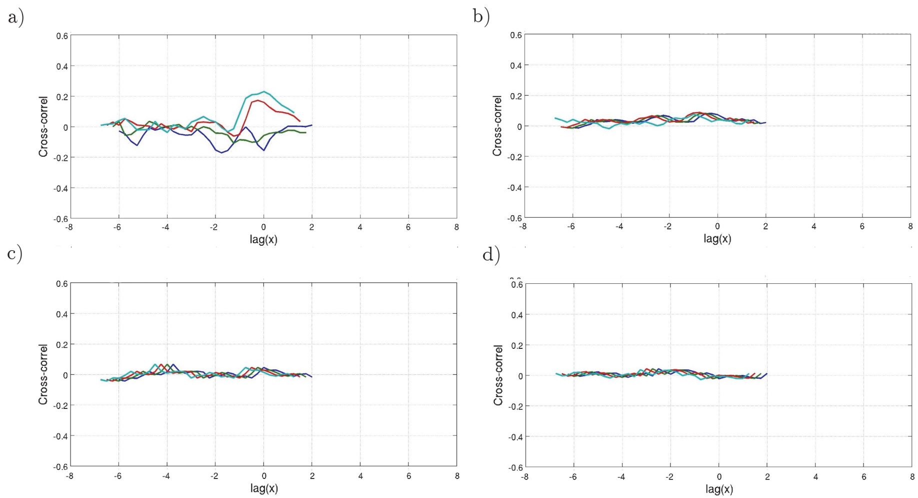

Fig. 7. *Y*–*C* cross-correlation at $t = 4\mathrm{T}$ for the nodes located at $y = 5.75\mathrm{L}$ in scenario 1a **(a)**, scenario 1b **(b)**, scenario 3a **(c)** and scenario 3b **(d)**. Each color corresponds to a correlation structure centered at a different node sampled by the plume (see Fig. 2b).

HESSD
9, 13083–13115, 2012

EnKF vs. ES for tracer test data assimilation

E. Crestani et al.

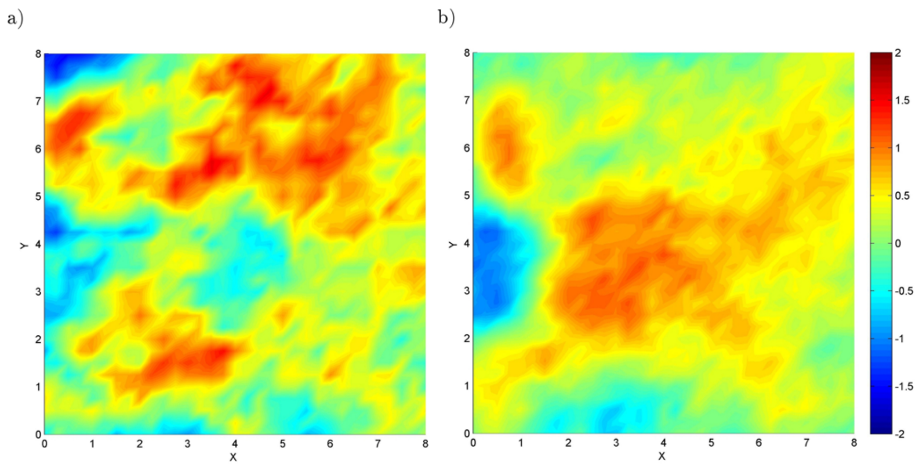

Fig. 8. Scenario 4: log-transformed hydraulic conductivity field retrieved by **(a)** EnKF and **(b)** ES assimilating concentration data transformed with a modified normal score transform. The color bar indicates log-transformed hydraulic conductivity in $\ln(\mathrm{L\,T^{-1}})$.

HESSD
9, 13083–13115, 2012

EnKF vs. ES for tracer test data assimilation

E. Crestani et al.

CC BY

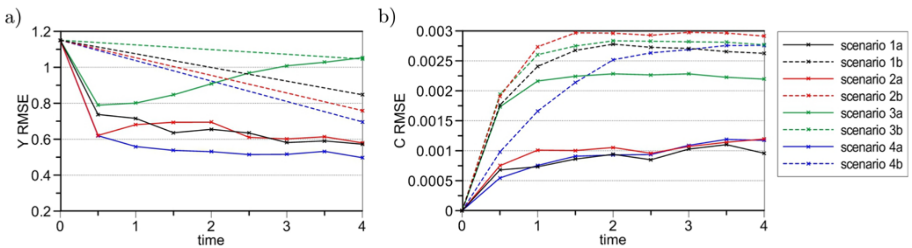

Fig. 9. Root mean square error of **(a)** the retrieved log-transformed hydraulic conductivity field and **(b)** the concentration distribution in the retrieved field for the all scenarios.

HESSD
9, 13083–13115, 2012

EnKF vs. ES for tracer test data assimilation

E. Crestani et al.

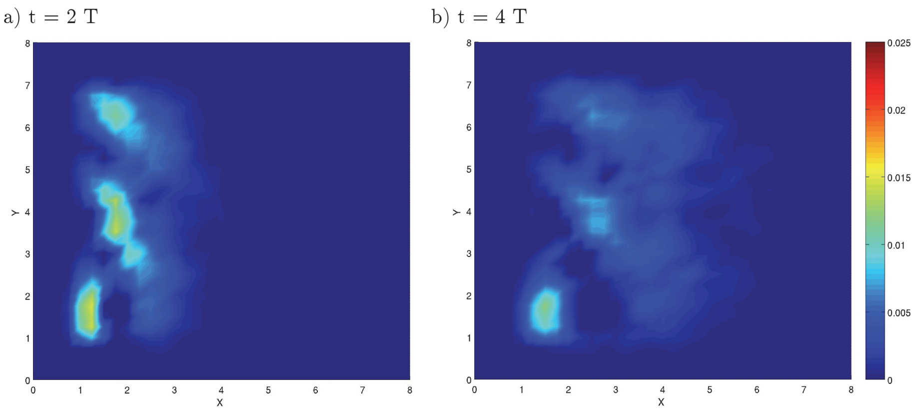

Fig. 10. Ensemble mean of the plume evolution at $t = 2\mathrm{T}$ and $t = 4\mathrm{T}$ in the prior Y fields. The color bar denotes concentration.

HESSD
9, 13083–13115, 2012

CC BY

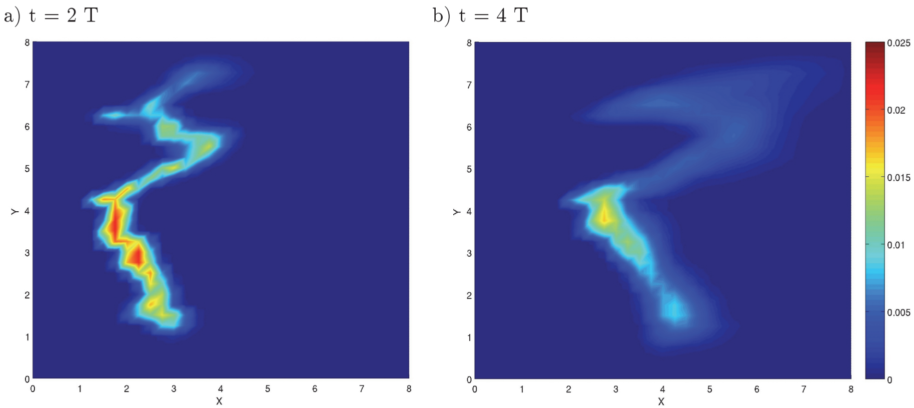

Fig. 11. Ensemble mean of the plume evolution at $t = 2\mathrm{T}$ and $t = 4\mathrm{T}$ in the Y field estimated at $t = 2\mathrm{T}$ by EnKF in scenario 1a. The color bar denotes concentration.

HESSD
9, 13083–13115, 2012

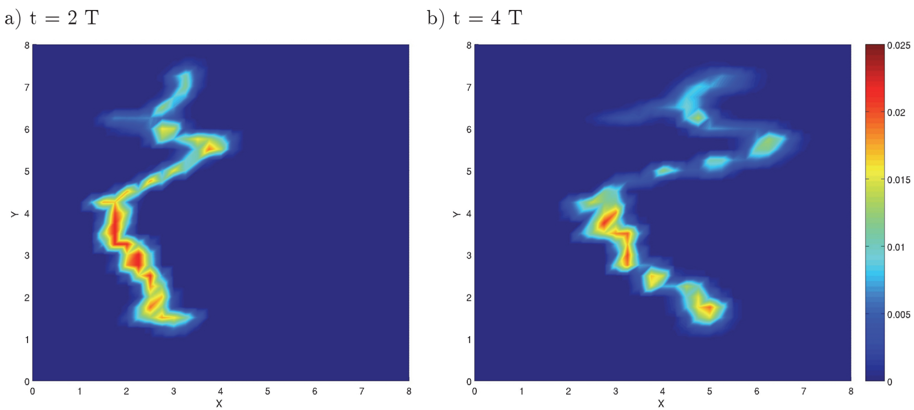

Fig. 12. Ensemble mean of the plume evolution at $t = 2\,T$ and $t = 4\,T$ in the Y field estimated at $t = 4\,T$ by EnKF in scenario 1a. The color bar denotes concentration.

HESSD
9, 13083–13115, 2012